DOI: 10.13009/EUCASS2023-431
Aerospace Europe Conference 2023 – 10TH EUCASS – 9TH CEAS

Aerodynamic and aerothermal comparison between the CAL1C and CAL1D geometries for the CALLISTO vehicle

Moritz Ertl[⋆†] *and Tobias Ecker*[⋆]
[⋆]*DLR – German Aerospace Center, AS-RFZ*
37073 Göttingen, Germany
moritz.ertl@dlr.de · tobias.ecker@dlr.de
[†]Corresponding author

Abstract

The "Cooperative Action Leading to Launcher Innovation in Stage Toss back Operations" (CALLISTO) is a cooperative project between DLR, JAXA and CNES for the research and development of reusable launch vehicle relevant technologies. Its goal is the development of a vertical take-off and vertical landing reusable subscale first stage demonstrator. The mission of the CALLISTO vehicle is to return to the launch pad using retro-propulsion and an Approach and Landing System (ALS) with deployable landing legs. This development leads to additional aerodynamic and aerothermal design questions compared to traditional launchers. An aerodynamic and an aerothermal database have been created to provide the relevant loads to system and product engineering teams. Since the creation of these databases the design process of the Callisto vehicle has matured and a new geometric shape of the vehicle has been designed. In this work we analyse the differences in aerodynamic and aerothermal loads between the geometries for two descent configurations. The simulations are done using Reynolds averaged Naiver Stokes methods with a Spalart-Allmaras turbulence model and frozen chemistry. We analyse the flow field as well as the surface distributions of coefficients and heat fluxes.

Keywords: reusable launcher, VTVL, retro-propulsion, Callisto, aerodynamic, aerothermal, database, reverse flight, CFD, RANS, geometry evolution

1. Introduction

Reusable launch vehicles have been of interest since last century[9] as a way of reducing launch costs. The recent successes of modern reusable concepts, such as SpaceX with their Falcon9 rocket,[1] have increased the interest in reusable launchers around the world. Europe and Japan are currently finalising the development of their new conventional launcher generation and have already started research and development on future concepts. The current European long term strategy aims at moving towards reusable launch vehicles (RLV) for the first stages of launchers. Part of this effort is the "Cooperative Action Leading to Launcher Innovation in Stage Toss back Operations"[3] (Callisto) - a cooperation between the German Aerospace Center (DLR), the Japan Aerospace Exploration Agency (JAXA) and the French Space Agency (CNES) to develop a flight demonstrator and the relevant technologies for future reusable launcher stages.

Callisto is a demonstrator for vertical take-off and vertical landing (VTVL) of a first stage of a space transport system. It has a single re-ignitable engine fueled with liquid hydrogen and oxygen. The mission is for the single stage to vertically launch and vertically return to the launch pad. The return flight has both phases of aerodynamic gliding - during which drag is used to break the vehicle - and of powered descend - during which the re-ignited engine is decelerating the vehicle for safe landing. When returning to the launch pad, the vehicle utilises its Approach and Landing System (ALS)[14] to deploy its landing legs.

Only few studies on the aerodynamics and aerothermodynamics of reusable VTVL launchers with powered decent exist, with no publications from existing launchers being known to the authors. In addition to the existing work on Callisto, aerothermal anlyses of theoretical retro-propulsion vehicles, covering the trajectory space for a full scale launcher have been conducted within the EU project RETALT[10] and the ESA project RETPRO.[2]

Aerodynamic and aerothermal databases have been generated to support the design process of the vehicle. The databases are utilised in many different aspects of the developments, from aerodynamic and thermal load predictions on specific components up to the design of the guidance and control system and overall mission design. In the case of reusable VTVL launchers, such as CALLISTO, the aerodynamic loads and the heat fluxes during powered descent are

DOI: 10.13009/EUCASS2023-431

of particular interest as they can not be inferred from conventional single use launcher knowledge. As an example, in the case of CALLISTO some of the highest heat fluxes are caused by heating of the aft bay section from hot exhaust gases getting pushed back due to the airflow. This especially affects the unfolded ALS during the final phase of the landing approach. The arising heat fluxes in turn influence the structural design and the thermal protection system (TPS) of the ALS.

Extensive databases for Callisto were generated by amalgamating wind tunnel data,[11] high fidelity CFD[4,5] and low fidelity CFD.[8] However, since the initial generation of the databases the development process of the Callisto vehicle has continued and the design of the vehicle has matured, resulting in a more detailed geometrical model. The creation of entirely new aerodynamic and aerothermal databases for the new geometry is considered too time consuming and too costly. Therefore, during the current stage of development, the task of the aero-science teams is twofold - to ensure the applicability of the existing databases and to further validate them.

In this paper we investigate the influence of a maturing geometry on the aerodynamic analysis of the Callisto vehicle. Two powered descent configurations, one with folded landing legs and one with deployed landing legs, are numerically simulated with high-fidelity computational fluid dynamics (CFD). We employ Reynolds averaged Naiver Stokes (RANS) with turbulence and chemistry modelling. The simulations are to provide a confirmation of the continued validity of the aerodynamic and aerothermal databases - based on an earlier design geometry - for the Callisto experimental flights with the evolved vehicle geometry.

2. Geometries, Configurations and Grids

Two vehicle geometries are investigated in this work. The CAL1C geometry is the first full 3D model of Callisto with regard to aerodynamic analyses. The databases for the aerodynamic and aerothermal loads are based on this geometry. It has been used for low fidelity and high fidelity CFD simulations and as wind tunnel model it has been investigated in three different wind tunnels.

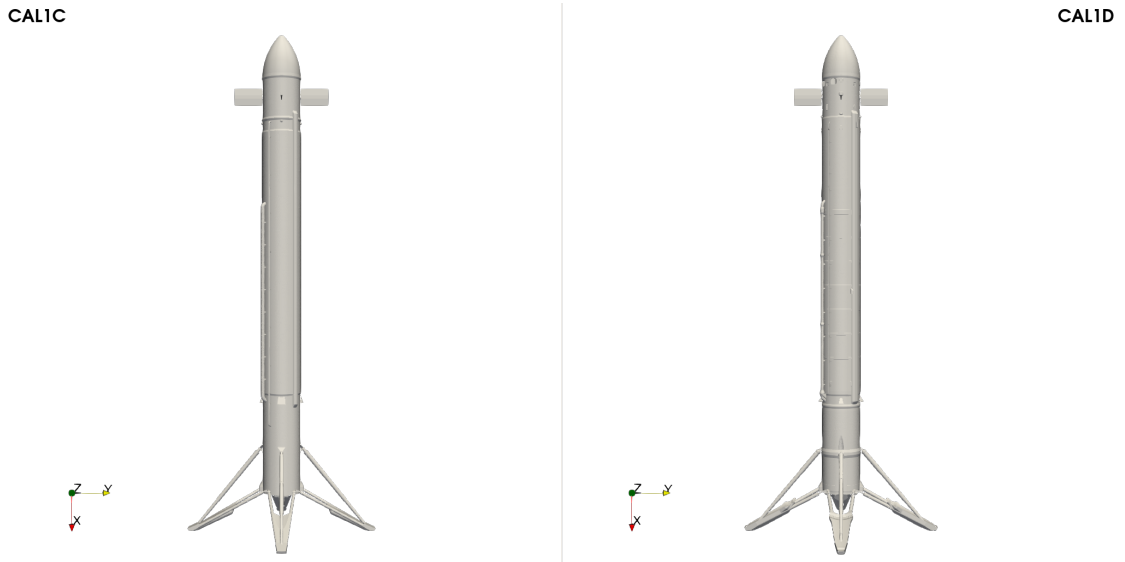

Figure 1: Full view of CAL1C and CAL1D geometries.

The CAL1D geometry is an evolution of the CAL1C geometry made necessary by a maturing of the design of the different vehicle parts. The changes in vehicle geometry between the CAL1C and CAL1D are as follows: The major parameters of the vehicle, such as the vehicle length $h \approx 13.450\,\text{m}$ and the diameter, which is also the reference length for aerodynamic coefficients, $D = L_{ref} = 1.1\,\text{m}$ remain the same. Also fin and leg positions in longitudinal (x-) direction are unchanged. The overall view of both geometries, therefore, is rather similar, as can be seen in fig 1.

An enlarged view of the upper sections is shown in fig 2. The main noticeable changes here are the additional protrusions and impressions on the vehicle equipment bay (VEB), just below the fairing. These are part of the reaction control system. The fins remain unchanged, but the fin lock mechanism has moved from the tank up onto the VEB structure.

A part of the H_2 tank is shown in fig 3. Here the CAL1D geometry has been enhanced with regular circular struts. Also visible are a change in diameter for some of the pressurisation pipes as well as a different fixture and an additional connector branching off from the cable duct.

DOI: 10.13009/EUCASS2023-431

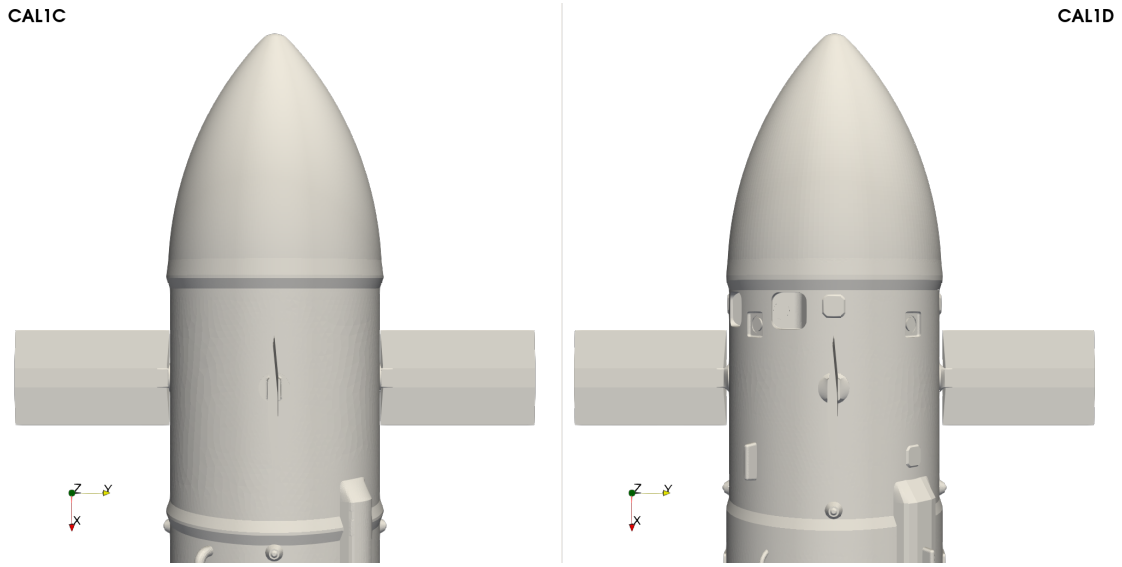

Figure 2: View of the fairing and vehicle equipment bay (VEB) of CAL1C and CAL1D geometries with additional protrusions and impressions in CAL1D.

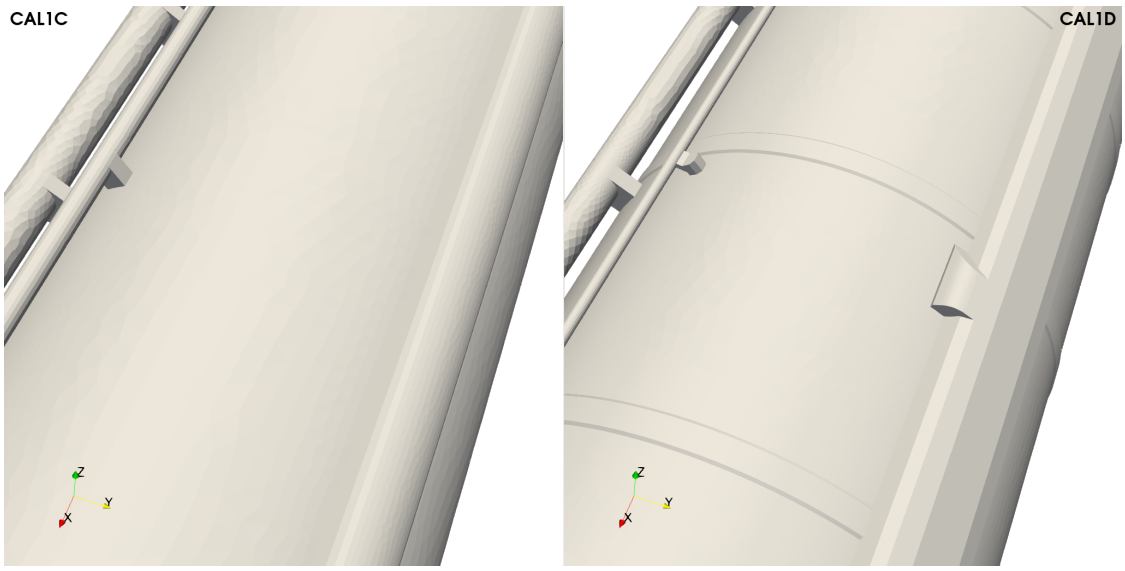

Figure 3: Section of the H_2 tank of CAL1C and CAL1D with additional circular struts and changes to piping and cable ducts.

The aft-bay with deployed landing legs is depicted in fig 4. The main change here is to the lower area of the landing legs, with a bulkier structure and a smoother surface. This redesign is due to the requirements of the thermal protection system. Also some differences in the nozzle gimbaling assembly and an additional covered flange connection for the aft-bay section are noticeable.

For this work we are presenting the analyses for two powered descent configurations of the Callisto demonstrator. The first is the UFO configuration, the configuration with deployed fins, folded landing legs and the engine switched on. It is used during the descent over a wide range of trajectory points. The second is the UUO configurations, with both fins and landing legs deployed and the engine switched on. It is used only during the very last part of the descent.

The increase in geometric details in the CAL1D geometry leads accordingly to an increase in necessary grid elements over the CAL1C mesh. A comparison between the grid is shown in fig 5. The computational grids for both configurations are similar. Two main differences can be observed. The CAL1C grid does not exhibit a grid refinement in front of the fairing. This is only the case in the UUO configuration and is not considered an issue since the UUO configuration is only operated in backward flight and thus the grid downstream of the vehicle should not affect

DOI: 10.13009/EUCASS2023-431

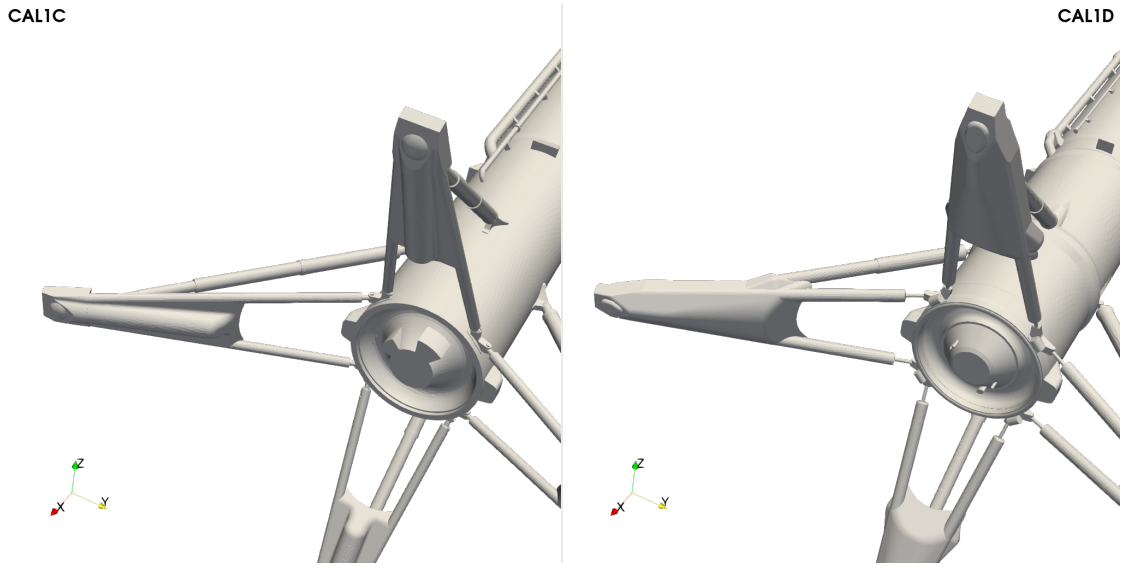

Figure 4: View of the aft-bay and deployed landing legs of CAL1C and CAL1D with differences in the nozzle gimbaling assembly and the landing leg geometry and an additional connecting flange.

the vehicle aerodynamics. For the UFO configuration the grid refinement in front of the fairing is used. The second difference is the use of a structured grid section in the plume region for CAL1C, which has been forgone for the CAL1D grid due to its impact on aerodynamics being considered low compared to the implementation effort. The amount of grid point has increased from 23 million in the case of CAL1C to 64 million for the CAL1D UFO configuration and to 86 million for the CAL1D UUO configuration.

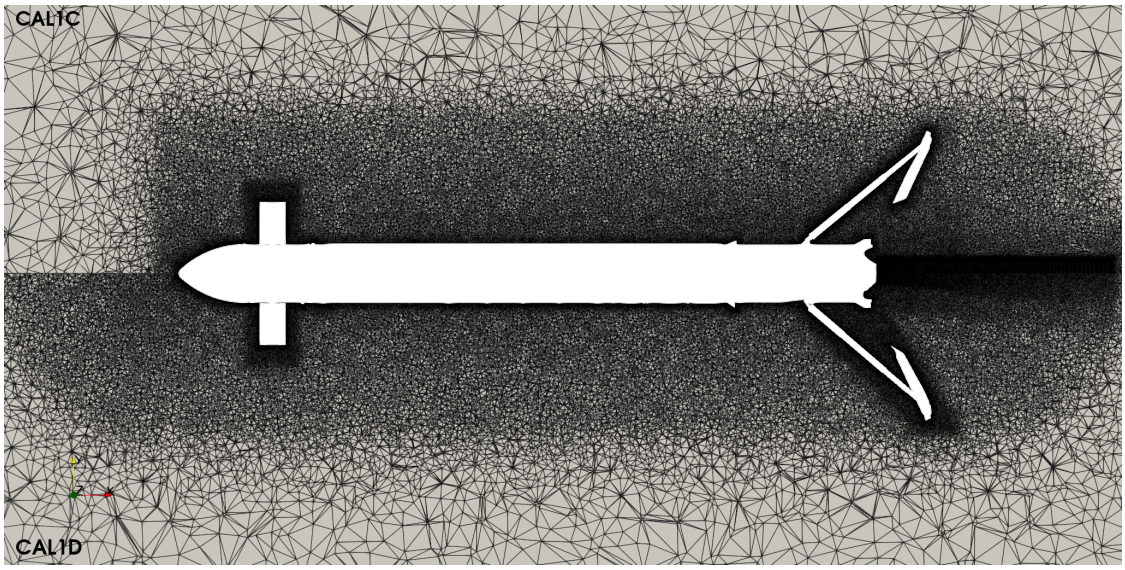

Figure 5: Comparative view of CAL1C and CAL1D computational grid.

3. Trajectory point selection

The creation of an entirely new set of databases for aerodynamic and aerothermal loads for the changed geometry - which has been discussed in the previous section 2 - was deemed too costly in both time and effort, within the scope of the Callisto project. Instead the chosen approach is to have a smaller number of additional simulations, done for select trajectory points. These simulations will then be used twofold, to investigate the differences between the two geometries and to contribute to the validation of the databases.

DOI: 10.13009/EUCASS2023-431

The trajectory points for CAL1D simulations have been chosen to either cover critical conditions, such as maximum dynamic pressure or to confirm flight phase relevant data, such as the landing drag. An overview of the simulated trajectory points is given in table 1. It is important to mention, that this list is not exhaustive for the validation simulations. As we are limiting ourselves to the powered descent, only the relevant trajectory points have been listed. A more in-depth description on the delta aerodynamics concept has been presented by Klevanski et al.[7]

Table 1: Investigated trajectory points for the comparison of CAL1C and CAL1D geometries.

Simulation ID	**Height** [m]	**Mach** [−]	**AoA** [°]	**AoR** [°]	**Thrust** [%]	**Config**
36	2600	0.7	165	0	110	UFO
27	2600	0.7	170	0	110	UFO
37	2600	0.7	175	0	110	UFO
26	2600	0.7	180	0	110	UFO
35	5000	0.8	170	0	110	UFO
28	5000	0.8	180	0	110	UFO
30	7100	0.9	180	0	110	UFO
	0	0.2335	180	0	40	UUO
	0	0.2335	155	0	40	UUO

4. Numerical Method and Setup

All simulations are done using the DLR TAU code.[6] The Tau code is solving the Reynolds averaged Navier-Stokes equations in a finite volume context on hybrid structured-unstructured meshes. In this work identical numerical methods and settings are used for the simulation of both geometries. The TAU code is used with a second order upwinding difference scheme AUSMDV[15] and least squares reconstruction for the gradients. For the temporal discretisation an explicit Runge-Kutta scheme with three stages is employed. To improve the computational accuracy for low Mach numbers, a modification of the variable reconstruction based on Thornber[13] is used. For the turbulence the one-equation Spalart-Allmaras[12] model is used as it provides the desired combination of stability, efficiency and accuracy for the database creation. The reasoning for the choice in turbulence model has been described in more detail in.[5]

For all simulations far field boundary conditions using the Mach number, angle of attack, angle of roll and density from the trajectory points are used together with a reference temperature of $T_\infty = 300\,\mathrm{K}$. All vehicle surfaces are treated as viscous walls with a wall temperature $T_{wall} = T_\infty = 300\,\mathrm{K}$. The plume is simulated with frozen chemistry as a two gas mixture between one species representing air and one representing the exhaust gas. The nozzle outflow is modeled as a Dirichlet boundary condition. For this condition the material properties for the "exhaust gas" mixture at combustion chamber conditions are obtained from a NASA CEA calculation for the hydrogen oxygen mixture. The velocity field and density and species distribution are obtained from a 2D nozzle simulation and are interpolated onto the 3D nozzle exit geometry. Two cases exist for the nozzle Dirichlet boundary condition, on with thrust level $Th = 110\%$ and one with $Th = 40$percent, which is used for the flight cases close to the ground with deployed landing legs. A more in depth description of the nozzle conditions and the Dirichlet boundary condition definition can be found in.[4]

5. Results

In the results section we will analyse select points for both the aerodynamic and the aerothermal influences of the matured design of the aero-shape of the Callisto vehicle. The analysed points are representative for the differences between the CAL1C and the CAL1D geometry which can be observed. To stay within the scope of reusable VTVL launchers we also limit ourselves to the powered reverse flight cases. In our results an angle of attack of 180° represents uninclined backward flight and in this case the inflow in the visualisations is coming from the right.

5.1 Aerodynamic comparison

In this section both global and local aerodynamic coefficients as well as the flow fields are analysed for the investigation into the congruence of the two geometries in the context of aerodynamics.

DOI: 10.13009/EUCASS2023-431

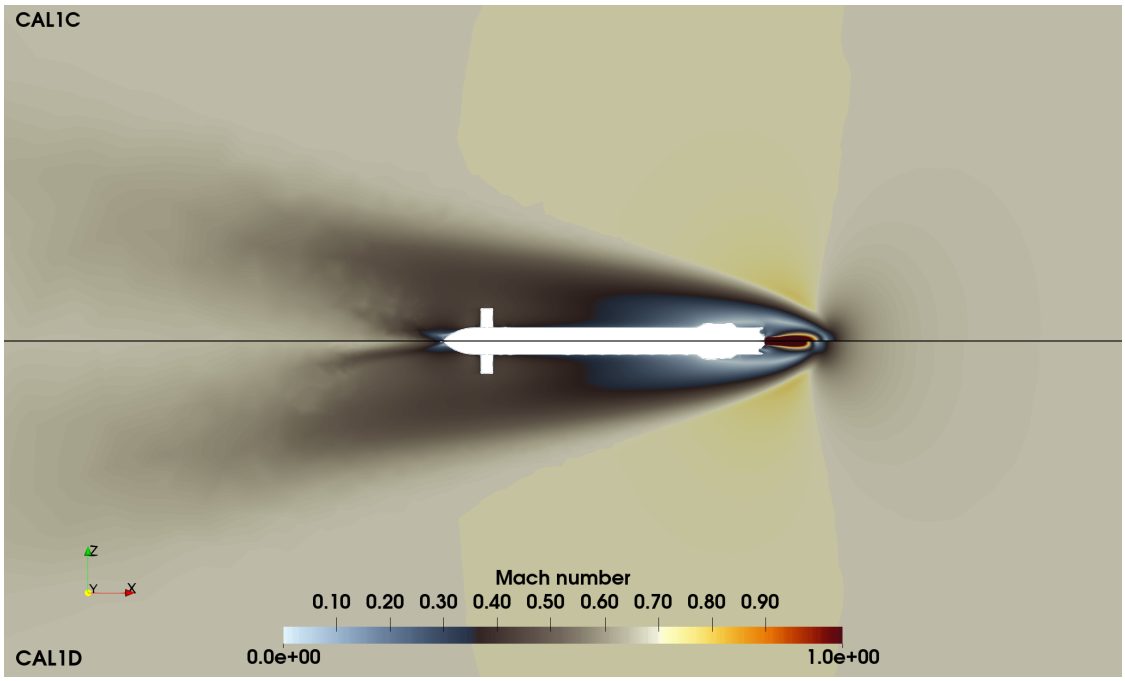

Figure 6: Comparative view of Mach number for UFO configuration (fins deployed, legs folded, engine on) for angle of attack $AoA = 170°$, $Ma = 0.7$ and thrust level $Th = 110\%$. CAL1C in upper half and CAL1D mirrored at x-axis in lower half.

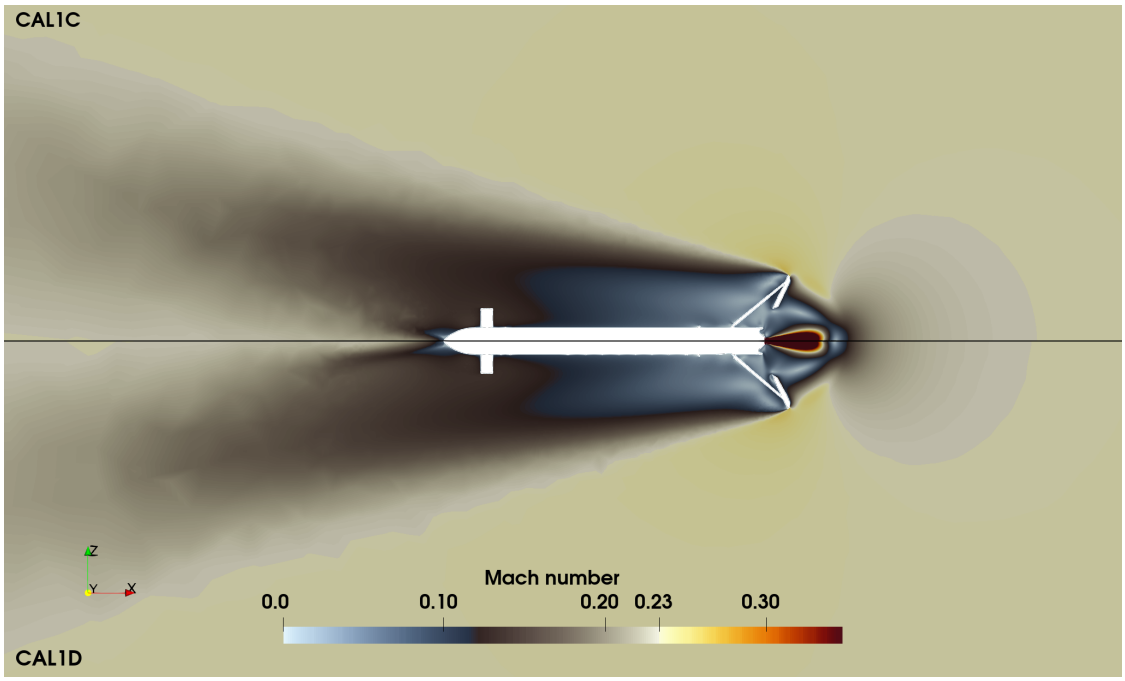

Figure 7: Comparative view of Mach number for UUO configuration (fins deployed, legs deployed, engine on) for angle of attack $AoA = 170°$, $Ma = 0.235$ and thrust level $Th = 40\%$. CAL1C in upper half and CAL1D mirrored at x-axis in lower half.

DOI: 10.13009/EUCASS2023-431

A visualisation of the flow field as Mach number plot for the UFO configuration for $Ma = 0.7$ and $AoA = 170\,°$ is given in fig 6 as a x - z - plane slice. To provide a good comparison the figure is split into an upper and a lower half, with the CAL1C result shown in the upper section and a mirrored view of the CAL1D result in the lower section. The flow fields are very similar at a first look. The overall shape of the flow field, with Mach numbers close to the far field $Ma = 0.7$ in areas upstream and far away from the vehicle, with a region of lower Mach number behind the plume, high velocities in the plume core and a clear wake area downstream of the vehicle. Some differences can be observed in the plume length, and the deceleration downstream of the fairing and the general intensity of the wake further downstream.

The observations are similar for the UUO configuration, which is shown for $Ma = 0.2335$ and the same $AoA = 170\,°$ in fig 7. The UUO configuration is only used during the last landing phase close to the ground and, therefore, always simulated with thrust level $Th = 40\%$. Here a larger wake is observed due to the deployed landing legs and the lower flight Mach number. The comparison between the two different geometries provides the same general points, with a slight difference in plume length, and downstream wake intensity. The reasons for the differences are most likely due to a combination of differences in the geometry and differences in the grids. Especially in the case of the plume length the above describe change from a structured section to an unstructured one is assumed to have some influence as well as the changes to the aft bay geometry. These differences are acceptable for our investigation since they contribute to the estimation of uncertainties from these sources.

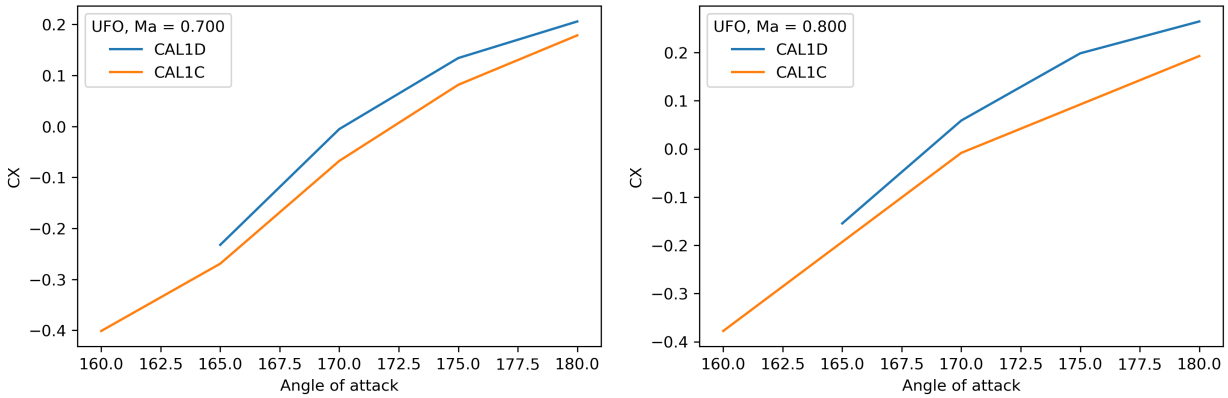

Figure 8: Comparison of global aerodynamic drag coefficient c_x over angle of attack between CAL1C and CAL1D geometries. UFO configuration for $Ma = 0.7$ on the left and $Ma = 0.8$ on the right.

For a more quantitative comparison we investigate differences in global aerodynamic coefficients. All coefficients have been analysed, but only the drag coefficient c_x is presented in this work as they exhibit the differences with the highest influence on the aerodynamic data base validity. While other coefficients, i.E. c_{Mx} do exhibit higher percentage differences, their absolute values are much lower. The global aerodynamic drag coefficients c_x for the UFO configuration for $Ma = 0.7$ and $Ma = 0.8$ and for different angles of attack are shown in fig 8 and for $Ma = 0.5$ in fig 9 on the left. The curves are in good agreement with the largest differences for $Ma = 0.7$ at $AoA = 170°$ with $\Delta c_x = 0.062$ and for $Ma = 0.8$ at $AoA = 180°$ with $\Delta c_x = 0.072$.

The global aerodynamic drag coefficients c_x for the UUO configuration for $Ma = 0.2335$ are shown in fig 8 on the right. For the UUO configuration, with deployed landing legs, the curves show a good agreement for higher angles of attack but exhibit increasing differences for $AoA = 170\,°$ and $AoA = 180\,°$ with a maximum of $\Delta c_x = 0.287$ at $AoA = 180\,°$.

These are good results for the UFO configuration. While differences between the two geometries exist, they are within the uncertainties defined in[7,8] for the CAL1C database. Therefore, the existing database keeps its validity. For the UFO configuration the differences are more pronounced and an investigation into the causes is prudent. To investigate the differences the local distribution of drag coefficient c_x over the length of the vehicle in longitudinal ($x-$) direction is plotted in fig 10, on the left, for the case of greatest difference in global values $AoA = 180\,°$.

The comparison of the local drag coefficient shows a very good agreement between the geometries for most of the vehicle. The c_x curves are nearly identical for $x = 0$ to $x = 12\,\text{m}$ and only exhibits minor differences up to $x = 14\,\text{m}$. The main deviation, with a $\Delta c_x > 0.25$ only occurs towards the end of the vehicle. A comparison of the drag coefficient, plotted onto the bottom surface of the landing legs, is given in fig 10 on the right for the investigated case. The simulation results have been cut along a center line, with the CAL1D results being shown in the upper half and the CAL1C results in the lower one. The visualisation reveals no major differences in the distributions, thus excluding changes in topology or the different plume resolution as causes for the difference in drag. The most likely causes are the increase in landing leg surface area for CAL1D combined with the changes to the geometry. This is supported by

DOI: 10.13009/EUCASS2023-431

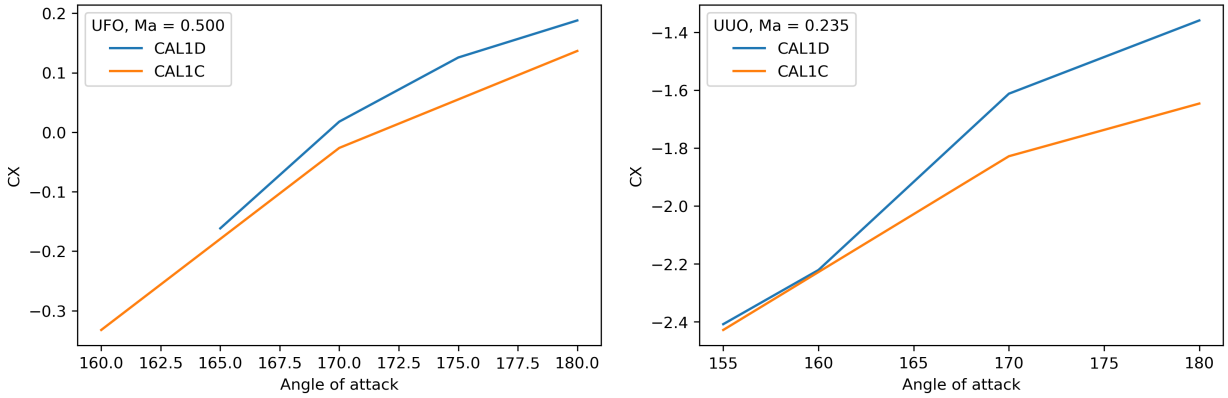

Figure 9: Comparison of global aerodynamic drag coefficient c_x over angle of attack between CAL1C and CAL1D geometries. UFO configuration for $Ma = 0.5$ on the left and UUO configuration for $Ma = 0.2335$ and $Th = 40\%$ on the right.

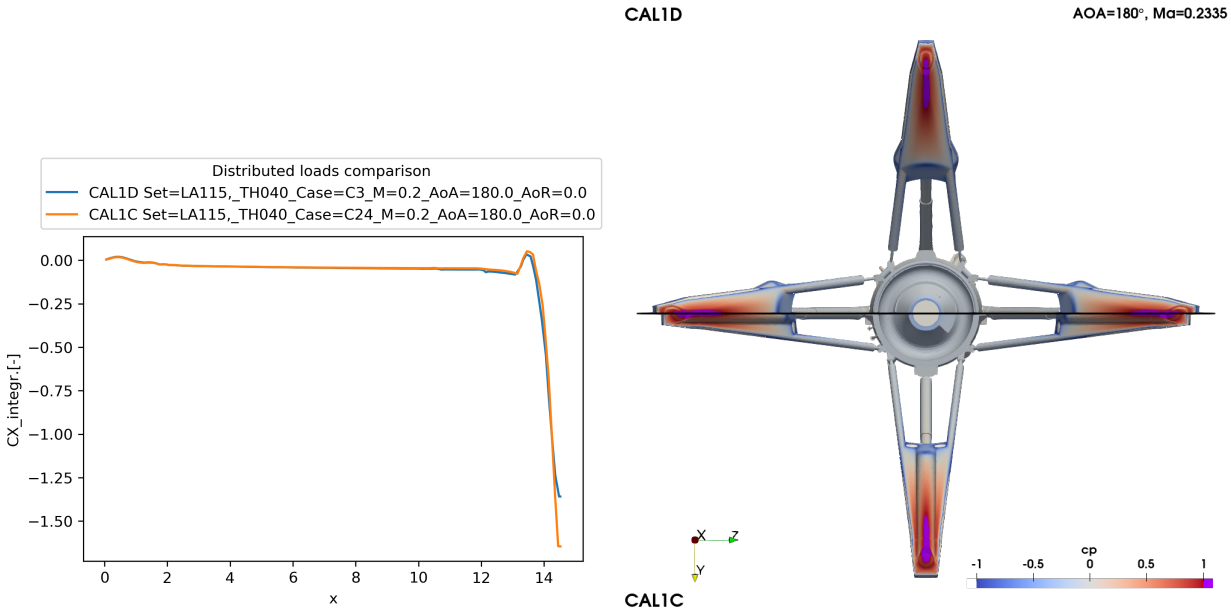

Figure 10: UUO configuration for $Ma = 0.2335$, $AoA = 180\,°$ and $Th = 40\%$. On the left: Comparison of local aerodynamic drag coefficient c_x distribution over the length of the vehicle in longitudinal ($x-$) direction between CAL1C and CAL1D geometries. On the right: Surface plot comparing the aerodynamic drag coefficient on the legs for half sections of CAL1C (bottom) and CAL1D (top).

the results of the UFO configuration, where the differences are smaller, as the landing legs are folded and thus have a much reduced influence. In the case of the UUO configuration an upward adjustment of the uncertainties is chosen to adapt the existing data base for continued use.

5.2 Aerothermal comparison

The aerothermal characterisation is an important aspect for defining the product requirements with regards to the thermal environment and TPS application. While the global geometric parameters between the different vehicle design phases have remained nearly constant, the CAL1D configuration has many small details added which are pertinent to the flight vehicle. The presented investigation is a preliminary study based on the high-fidelity aerodynamic simulation data, with a more dedicated study to follow.

DOI: 10.13009/EUCASS2023-431

5.2.1 Local comparison of UUO and UFO configuration thermal loads

A visualisation of the surface heat flux is given in fig 11 for UUO configuration for the trajectory point $Ma = 0.2335$, $AoA = 170\,°$ and $Th = 40\%$. There are three different views given, a bottom view of the base and the landing legs on the left, a y-x side view in the middle and a z-x side view on the right. For comparison between CAL1C and CAL1D, the simulation results for the two geometries have been cut in a central plane and reassembled from two halves for each view. The surfaces were simulated as isothermal walls with a wall temperature of $T_w = 300\,\mathrm{K}$.

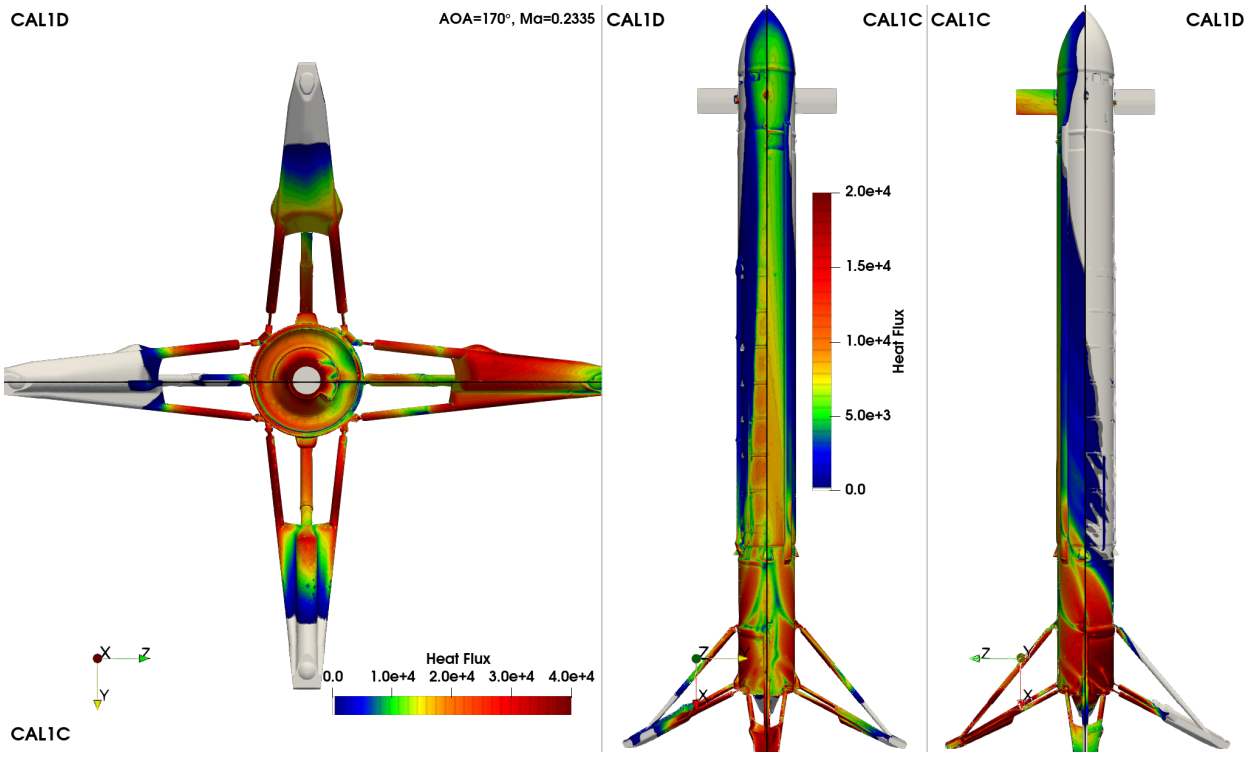

Figure 11: Heat flux surface comparison. UUO configuration $Ma = 0.2335$, $AoA = 170\,°$ and $Th = 40\%$. Left: bottom view of the base section and landing legs, AoA directed to the right. Middle: y-x side view, AoA directed into the view plane. Right: z-x side view, AoA directed to the left.

An initial visual comparison of the heat fluxes of the CAL1C and CAL1D geometries shows an overall agreement. The regions of high and low heat flux are congruent in all three views. Three major differences can be observed. The addition of the circular struts on the tank surface for CAL1D, which are shown in more detail in fig 3, leads to a more discrete heat flux distribution with hot spots in between two strut segments, which can be observed in fig 11 in the middle. The additional flange at the aft-bay, which is shown in fig 4, leads to a reduction of the heat flux upstream, which is especially visible on the leeward side, in fig 11 on the right. The landing leg geometry has not only slightly increased in size, but also in shape. The pronounced cylindrical foot pad of the CAL1C geometry has been changed to a smoother lower section. The effect of this leg geometry change on the heat flux can be observed in fig 11 on the left with a reduced maximum on the foot pad in the y-direction.

5.2.2 Global comparison of UFO configuration thermal loads on system interface level

The general idea and the concept of the CALLISTO aerothermal database is described in detail in.[4] For the purpose of this study the thermal loads on the interfaces of the aerodynamic database flight points are evaluated for both CAL1C and CAL1D UFO configuration computations.

Some of the many interfaces (36 and more depending on product application) defined during grid generation are shown in figure 12. For comparison of several flight cases (as shown in table 1, all double digit cases) the average heat flux on selected interfaces is computed for both CAL1C and CAL1D configurations. The results are shown in figure 13. The first four flight conditions are at M = 0.7 at varying angles of attack (165 - 180 deg). The influence of the angle of attack is very distinct, especially for interfaces close to the vehicle nose or protruding interfaces like the fins (displayed is fin 1). At smaller angles of attack the exhaust plume only partially submerges the vehicle, leading to lower thermal loads on these interfaces. Interfaces close to the base plate do not show a strong dependency on the angle of attack as

DOI: 10.13009/EUCASS2023-431

they are local to the nozzle exit and plume deflection is minimal. Generally the comparison of interface thermal loads shows a good agreement between both aeroshapes indicating the applicability of the CAL1C aerothermal database for later aeroshape iterations and product requirements.

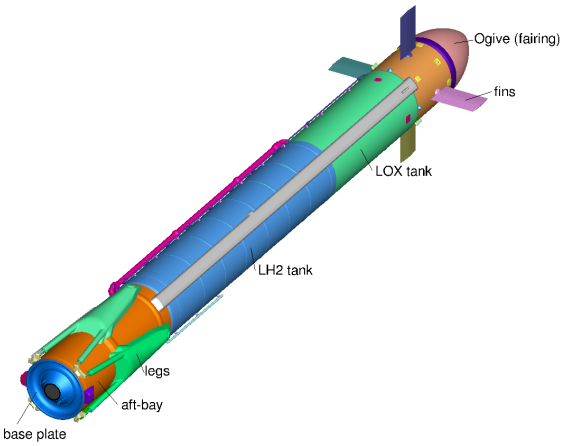

Figure 12: Visualisation of thermal interfaces for UFO configuration. Selected interfaces are named.

6. Conclusion

We investigated the effects of a geometry design evolution on the aerodynamic and aerothermal databases for a reusable first stage VTVL demonstrator. The work is done in the context of the Callisto vehicle, a cooperation between DLR, CNES and JAXA. While the original databases were created from a combination of wind tunnel data and low fidelity and high fidelity CFD data, this analysis limits itself to comparisons of high fidelity CFD simulation for cases during descent with an active engine. Generating entirely new databases for the updated geometry is deemed to costly in both time and effort and thus a limited selection of trajectory points relevant to mission and systems is investigated. The simulations are done with the DLR TAU code, solving Reynolds averaged Navier Stokes equations on finite volumes.

An analysis of the aerodynamic coefficients and the flow field reveals generally small differences between for the updated aeroshape. This is unsurprising as most of the changes to the geometry are also minor. The largest differences were observed in the case of the landing configuration UUO with deployed legs. For the landing legs the changes to the geometry are most pronounced and occur in combination with an increase in surface area. For most configurations the differences are within the uncertainties of the existing database. For the configuration with deployed landing legs an adaptation of the uncertainty range will be applied. This allows for the continued application of the aerodynamic database to the updated geometry.

A preliminary investigation into the aerothermal aspects of the geometry evolution provides results consistent with aerodynamics. Visualisations of the surface heat flux show a similar distribution for both geometries. Local differences are connected to radial struts on the tanks, an additional flange at the aft-bay and geometry changes to the landing legs. An investigation of the area averaged integral heat fluxes on the vehicle sections used in the database, however, exhibits only minor differences over the investigated flight conditions. The validity of the existing aerothermal database for the updated geometry is given, though a discussion with affected products on the relevance of the local differences is warranted.

7. Acknowledgments

The authors would like to thank Josef Klevanski for the treatment of the CAD models and for leading the DLR aero science team for Callisto. The authors would like to thank Bodo Reimann for support with the grid generation. The authors would like to thank Sven Krummen, Johannes Riehmer, Etienne Dumont, Jean Desmariaux and Florent Puel for fruitful discussions. The authors would like to acknowledge the DLR and the Callisto project for the funding.

DOI: 10.13009/EUCASS2023-431

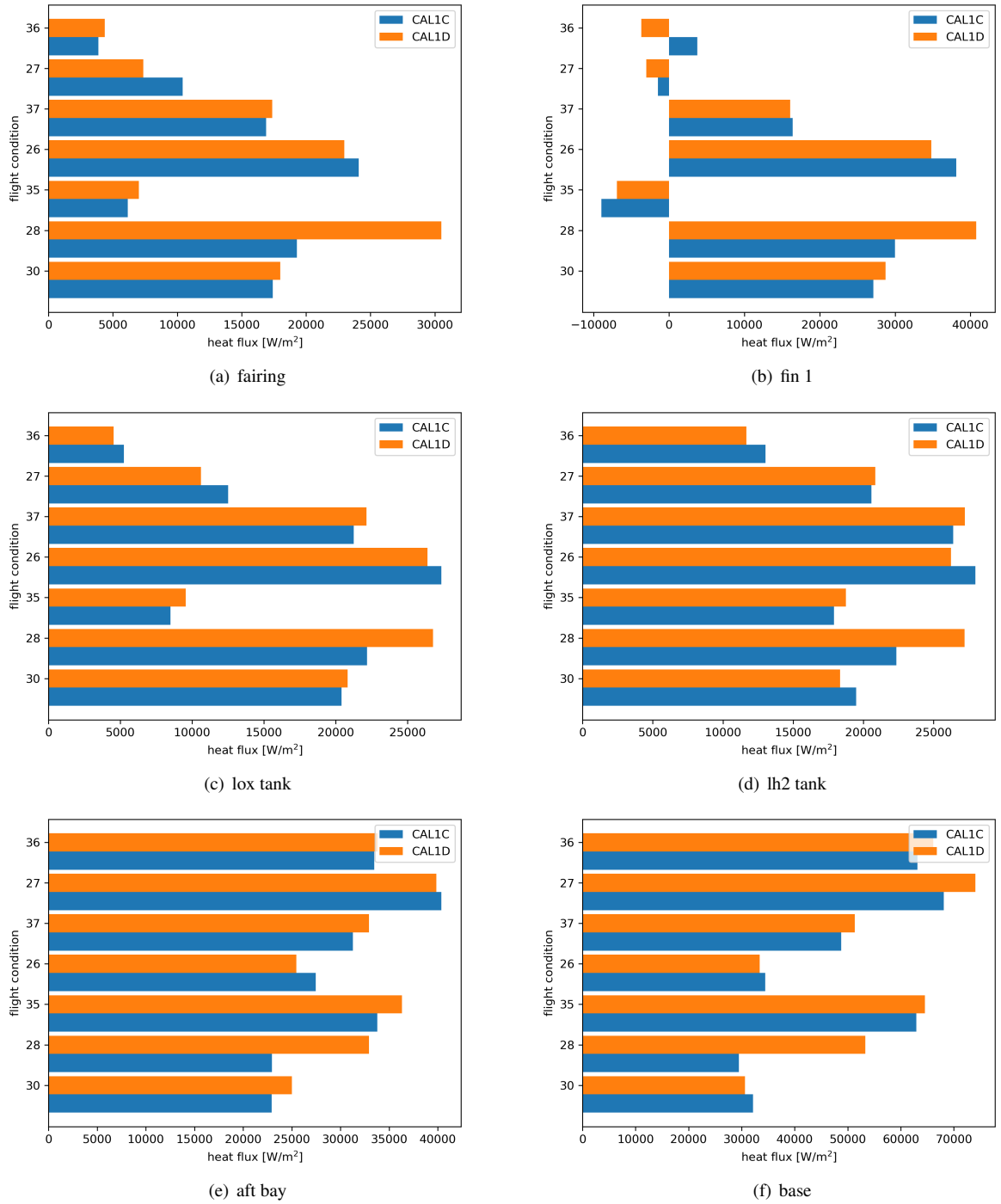

(a) fairing

(b) fin 1

(c) lox tank

(d) lh2 tank

(e) aft bay

(f) base

Figure 13: Comparison of average heat fluxes on for selected interfaces for both UFO CAL1C and CAL1D configuration. Flight conditions reference to table 1.

References

[1] Lars Blackmore. *Frontiers of Engineering: Reports on Leading-Edge Engineering from the 2016 Symposium*, chapter Autonomous Precision Landingof Space Rockets, pages 33–41. The National Academies Press, Washington, DC, 2017.

[2] Tamas Bykerk, Daniel Kirchheck, and Sebastian Karl. Reconstruction of wind tunnel tests using cfd for a reusable first stage during rocket retro-propulsion. In EUCASS, editor, *9th European Conference for Aeronautics and Space Sciences (EUCASS) 2022*, pages 1–14, July 2022.

DOI: 10.13009/EUCASS2023-431

[3] Etienne Dumont, Shinji Ishimoto, Pascal Tatiossian, Josef Klevanski, Bodo Reimann, Tobias Ecker, Lars Witte, Johannes Riehmer, Marco Sagliano, Sofia Giagkozoglou Vincenzino, Ivaylo Petkov, Waldemar Rotärmel, René Schwarz, David Seelbinder, Markus Markgraf, Jan Sommer, Dennis Pfau, and Hauke Martens. Callisto: a demonstrator for reusable launcher key technologies. In *32nd International Symposium on Space Technology and Science (ISTS)*, Fukui, Japan, June 2019.

[4] Tobias Ecker, Moritz Ertl, Joseph Klevanski, Etienne Dumont, and Sven Krummen. Aerothermal characterization of the callisto vehicle during descent. In *9th European Conference for Aeronautics and Space Sciences*, 2022.

[5] Moritz Ertl, Tobias Ecker, Joseph Klevanski, Sven Krummen, and Etienne Dumont. Aerothermal analysis of plume interaction with deployed landing legs of the callisto vehicle. In *9th European Conference for Aeronautics and Space Sciences*, 2022.

[6] Klaus Hanemann, Jan M. Schramm, Alexander Wagner, Sebastian Karl, and Volker Hanemann. A closely coupled experimental and numerical approach for hypersonic and high enthalpy flow investigations utilising the heg shock tunnel and the dlr tau code. Technical report, 2010.

[7] Josef Klevanski, Sven Krummen Bodo Reimann, Moritz Ertl, Tobias Ecker, Johannes Riehmer, Etienne Dumont, Lâle Evrim Briese, and Thiemo Matthias Kier. Further progress in aerodynamic studies for callisto - reusable vtvl launcher first stage demonstrator. In *Aerospace Europe Conference 2023 – 10TH EUCASS – 9TH CEA*, 2023.

[8] Josef Klevanski, Bodo Reimann, Sven Krummen, Moritz Ertl, Tobias Ecker, Johannes Riehmer, and Etienne Dumont. Progress in aerodynamic studies for callisto - reusable vtvl launcher first stage demonstrator. In *9th European Conference for Aeronautics and Space Sciences*, June 2022.

[9] D.E. Koelle and H. Kuczera. Sänger ii, an advanced launcher system for europe. *Acta Astronautica*, 19(1):63 – 72, 1989.

[10] Mariasole Laureti and Sebastian Karl. Aerothermal databases and load predictions for retro propulsion-assisted launch vehicles (retalt). *CEAS Space Journal*, 2022.

[11] J. Riehmer, K. Kapteijn, J. Klevanski, B. Reimann, A. Gülhan, and E. Dumont. Wind tunnel experiments of the callisto vtvl launcher in the tmk and hst wind tunnels. In *9th European Conference for Aeronautics and Space Sciences*, 2022.

[12] P. Spalart and S. Allmaras. *A one-equation turbulence model for aerodynamic flows*. 1994.

[13] B. Thornber, A. Mosedale, D. Drikakis, D. Youngs, and R.J.R. Williams. An improved reconstruction method for compressible flows with low mach number features. *Journal of Computational Physics*, 227(10):4873–4894, 2008.

[14] Sofia Giagkozoglou Vincenzino, Silas Eichel, Waldemar Rotärmel, Felix Krziwanie, Ivaylo Petkov, Etienne Dumont, Anton Schneider, Silvio Schröder, Jens Windelberg, Tobias Ecker, and Moritz Ertl. Development of reusable structures and mechanisms for callisto. In *33rd ISTS Conference*, March 2022.

[15] Yasuhiro Wada and Meng-Sing Liou. A flux splitting scheme with high-resolution and robustness for discontinuities. In *32nd Aerospace Sciences Meeting and Exhibit*, 1994.